11th International Symposium on Magnetic Bearings
August 26-29, Nara, Japan

LINEAR MAGNETIC BEARING/ACTUATOR DESIGN AND PROTOTYPE FOR PRECISION SPINDLES

Xiaodong Lu, Matthew Paone, Irfan-ur-rab Usman
Department of Mechanical Engineering, The University of British Columbia
Vancouver, British Columbia, V6T 1Z4, Canada, xdlu@mech.ubc.ca

Alexander Slocum
Department of Mechanical Engineering, Massachusetts Institute of Technology
Cambridge, Massachusetts, 02139, USA, slocum@mit.edu

ABSTRACT
In precision manufacturing, magnetic thrust bearings can be advantageously used to provide both high axial stiffness and short-stroke axial in-feed motion for precision spindles. This paper presents the design, analysis, prototype, and experimental results of a compact radially-biased magnetic thrust bearing with linear force characteristics. The first prototype of the thrust magnetic bearing demonstrates less than 5 nm RMS positioning noise over 1 mm stroke and 1500 Hz closed-loop bandwidth. The actuating force is over 300 N at continuous working condition and a maximum of 600 N.

INTRODUCTION
Generally, machine tools require stiffer structural loops and fewer components to increase accuracy and reduce cost. Precision machine tool spindles are typically supported with thrust bearings on a Z axis slide, which requires another actuator to provide axial in-feed motion. A fundamentally new approach to address this issue is to use magnetic thrust bearings as actuators to provide several millimeters of Z stroke required for meso machining and face grinding, and thus a separate Z-axis slide is no longer needed, which results better accuracy, higher stiffness and lower cost.

Existing solutions to Z-axis actuating include moving magnet motors and conventional push-pull magnetic bearings. Zhang et al described a magnetically levitated spindle for Micro EDM machining [1]. This moving-magnet axial actuator achieved 2 mm axial stroke, 0.5 μm resolution, and 110 Hz bandwidth. A similar technology is applied in an aerostatic spindle for micro-milling to achieve 10 mm axial stroke and 174 Hz bandwidth [2]. Liebman constructed a rotary-linear hybrid axis for meso-scale machining [3]. This machine used a linear motor as axial actuator, which had 25 mm linear travel, 2.5 nm positioning noise, and 70Hz bandwidth [3]. These Lorentz-motor based designs can easily achieve fairly large axial stroke up to tens of millimeter, but the force density is much less than solenoid type normal-stress magnetic bearings.

A normal-stress magnetic bearing force is in a normal direction to the stator/rotor pole surface with a surface density of $B^2/2\mu_0$ N/m^2, where B is flux density in Tesla and $\mu_0=4\pi\times10^{-7}$ is the magnetic permeability of air. However, the conventional push-pull type magnetic bearings have a highly-nonlinear characteristic, which not only deteriorates the axial position control accuracy, but also makes the actuator very inefficient at large air gaps. Biasing currents are usually applied to improve linearity for constant position regulation, which doesn't work well over large air gap variation during axial travel. Permanent magnets have been used in magnetic bearings to generate bias flux and improve linearity, such as radial magnetic bearings [4], planar suspension stages [5], and thrust bearings [6]. In these designs, a significant portion of the thrust pole face area opposes the coil windings and cannot contribute to force generation. In addition, unnecessarily large armature plate can introduce vibration modes and limit the achievable bandwidth.

To address these issues, this paper presents the design, prototyping, and experimental results of a spatially-compact electromagnetic actuator used for precision spindle thrust bearing and axial motor.

LINEAR MAGNETIC ACTUATOR DESIGN CONCEPT
Figure 1 shows the layout of the permanent magnet biased bearing/actuator design, which is the axis symmetric version of the ultra-fast tool servo actuator [7]. The linear bearing/actuator is made of four main components: a ring-shaped permanent magnet, two excitation coils, three piece stator cores, and an armature. Both the stator and armature are made of soft magnetic materials. The permanent magnet ring is radially magnetized as indicated by the red arrows in the A-A cross-section of Figure 1. There is a small opening in the ring as indicated by the black line to avoid the eddy current induced along the azimuthal direction during transient state, as the rare earth magnet is a good conductor. This magnet produces two linearizing bias fluxes (solid lines) which flow into the armature and return through each half of the stator core. Two coil

windings fit into the empty slots in the stator and they can be driven in serial. This current produces an excitation flux (dotted line) traveling only through the stator and armature. This excitation flux can change the normal fluxes on the left and right surfaces of the armature. As a result, the normal force density on the armature pole face is altered by the excitation flux. The axial air gap between the armature and the stator pole surface sets the maximum stroke of the actuator in the axial direction. There is a radial air gap between the magnet and the armature to ensure contact free motion. The axis symmetric homopolar design ensures that there are no eddy currents induced by the spindle shaft rotary motion.

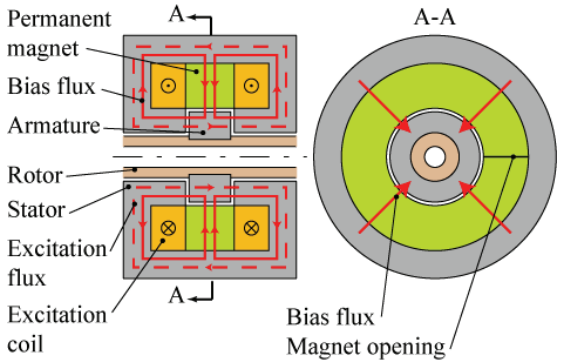

FIGURE 1: The schematic diagram of the magnetic bearing/actuator design.

FORCE ANALYSIS

The force analysis of the magnetic bearing can be broken down into two parts: a bias flux analysis which examines the flux generated by the permanent magnet, and an excitation flux analysis which examines the contributions from the excitation coils. In the end, the bias and excitation components will be brought together and an expression for the force will be derived. Here we assume that the permeability of the armature and stator cores is infinite and leakage fluxes are negligible.

Given that the total air gap is $2x_0$ and the armature axial displacement is x off the center position, the air gap to the right of the armature is denoted as $x_0 - x$, the gap on the left as $x_0 + x$, and the bias flux density in each of these gaps is $\overline{B}_1$ and $\overline{B}_2$ respectively. The bias flux from the magnets is the remanence B_r multiplied by the magnet pole area A_{PM}. Applying Gauss' law to a surface surrounding the armature and neglecting leakage, we have:

$$\left(\overline{B}_1 + \overline{B}_2\right)A - B_r A_{PM} = 0\,, \tag{1}$$

where A is the stator pole area. Applying Ampere's law and combining with (1) we have:

$$\overline{B}_1 = \frac{B_r A_{PM}}{2A}\left(\frac{x_o + x}{x_o}\right), \text{ and } \overline{B}_2 = \frac{B_r A_{PM}}{2A}\left(\frac{x_o - x}{x_o}\right). \tag{2}$$

When driven with current i, the two coils with a combined N turns produce the excitation flux:

$$\widetilde{B} = \frac{N\mu_0}{2x_o} i\,. \tag{3}$$

Using the principle of superposition, the total flux in each air gap is:

$$B_1 = \widetilde{B} + \overline{B}_1\,, \tag{4}$$

$$B_2 = \widetilde{B} - \overline{B}_2\,. \tag{5}$$

Summing the magnetic forces on the armature, gives the total actuating force in the axial direction:

$$F(x,i) = \frac{A\overline{B}}{\mu_o x_o}\left(2\overline{B}x + \mu_o N i\right) \tag{6}$$

This can be rewritten as:

$$F(x,i) = k_x x + k_i i \tag{7}$$

where we refer k_x as the bearing stiffness and k_i as the bearing force constant. The linear force characteristic is desirable for applications requiring very high precision. In comparison with current-biased conventional push-pull magnetic bearing, the required coil winding area of this design is 25% and the generated heat is 50% of a conventional magnetic bearing, given the same stroke and force requirement.

Combining the actuator force expression with the rotor mechanical model and neglecting friction on the rotor shaft, the transfer function from the actuating current to the axial displacement can be represented as:

$$\frac{x(s)}{i(s)} = \frac{k_i}{ms^2 - k_x}\,. \tag{8}$$

FINITE ELEMENT MODELLING

Analytical force expression can give intuitive understanding on the actuator working principle, but it is hard to consider such effects as finite permeability of magnetic materials and leakage fluxes. In order to model these effects, 2-D finite element analysis software FEMM [8] is used in the axis-symmetric mode to investigate the force characteristics of a prototype design. Table 1 lists the key parameters of the linear bearing/actuator prototype. The soft magnetic material is Somaloy powdered iron from Höganäs [9] to improve

the high frequency performance due to its insulation coating around fine iron powers. The maximum permeability is 500, according to the material datasheet. The soft magnetic material of the stators and the armature was modeled with the B-H curve provided by the material manufacturer, which includes non-linearity and saturation effects. The permanent magnet is 44 MGOe rare earth NdFeB magnet.

TABLE 1: Prototype actuator parameters

Parameter	Value
Armature outer diameter	49.8 mm
Armature thickness	12.7 mm
Stator pole inner diameter	27.9 mm
Stator pole outer diameter	48.0 mm
Coil winding inner diameter	48.0 mm
Coil winding outer diameter	80.0 mm
Coil winding thickness	20.0 mm
Magnet inner diameter	50.8 mm
Magnet outer diameter	80.0 mm
Magnet thickness	13.9 mm
Stator pole face area	1198 mm^2
Nominal axial air gap, x_0	1.22 mm
Coil turn number each side	112 turns
Magnet remanence	1.326 T
Radial air gap	0.508 mm
Axial Stroke Length	1 mm

Figure 2(a) shows the bias flux distribution inside the actuator when the armature is in the center position and the excitation current is zero. Figure 2(b) shows the flux distribution when the excitation current rises to 2.6 A and the armature is still at the center. By comparison, the excitation current steers a portion of the permanent magnet flux from the left side to the right side of the armature and thus a net actuating force is generated towards to the right side. Figure 2(c) shows the flux distribution when the armature is positioned to the right end and the excitation current is zero. The armature displacement shifts the flux from the left to the right, which generate a force further enhance the displacement. As derived in (9), this negative stiffness effect brings a right-half-plane pole, which sets the lower limit of the achievable bandwidth the closed loop axial motion system. By investigating the total actuating force at various armature positions and excitation current levels, the FEA gives us k_x = 1.53 N/μm, and k_i = 147 N/A, which will be later compared with experimental measurements.

MAGNETIC BEARING PROTOTYPE

A prototype with design parameters in Table 1 is built and integrated into a commercial air-bearing spindle to test the performance of this magnetic actuator. As shown in Figure 3, the original aerostatic thrust bearing is replaced with the magnetic bearing prototype, while the two radial aerostatic bearings are retained. The armature is installed on the spindle shaft assembly. The magnetic bearing stator section is split into three assemblies: the front stator assembly, the middle stator assembly, and the rear stator assembly. A capacitance displacement sensor with 1-mm range is installed at the rear end of the spindle for the axial position feedback.

Figure 4 shows the spindle shaft assembly, on which installed from the left side to the right are aerostatic radial bearing, brushless rotary motor magnet, magnetic actuator armature, locknut, and a flat screw as capacitance displacement sensor target surface.

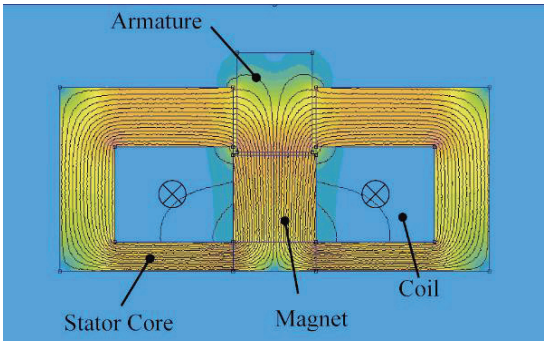

(a) $x = 0$, $i = 0$

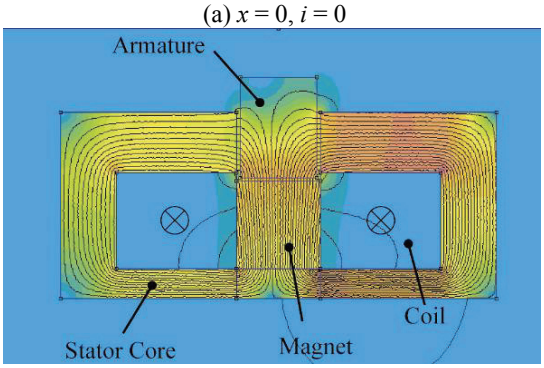

(b) $x = 0$, $i = 2.6$A

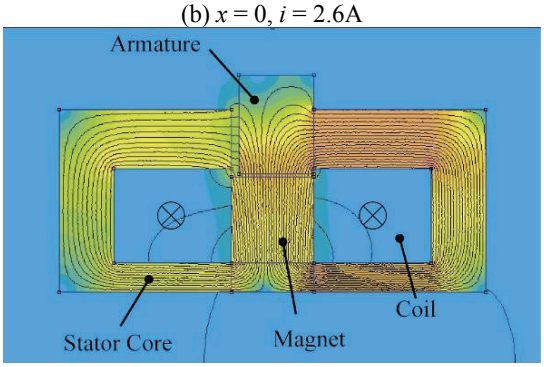

(c) $x = x_0$, $i = 0$

FIGURE 2: Flux distribution from finite element analysis.

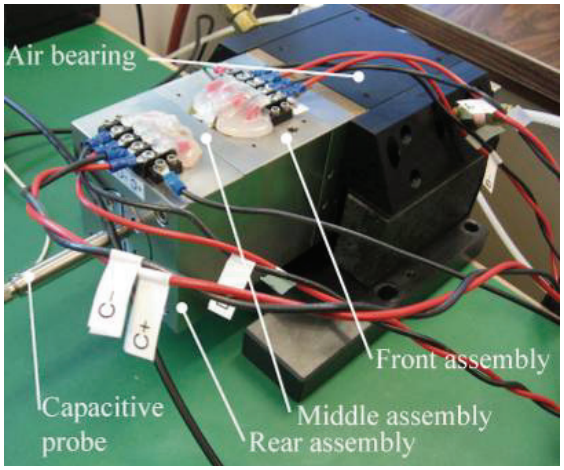

FIGURE 3: The spindle assembly with the prototyped axial actuator.

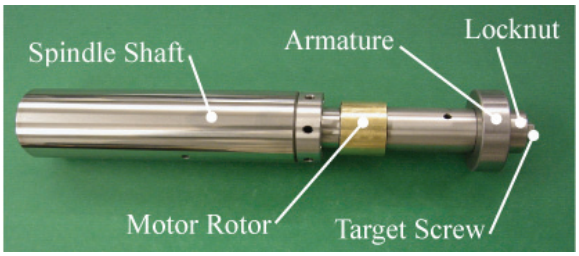

FIGURE 4: The spindle shaft assembly.

Figure 5 shows the fabrication of the front stator assembly, which is composed of a stainless steel frame, the stator cores, and the coil winding. The stator cores are split into four pieces and then epoxied together into the stator frame, mainly due to the available blank size of the power-pressed iron. The coil winding is made of a stack of pancake-shaped minor coils, which are interconnected together. Eventually, epoxy is applied to cover the whole coil winding and the whole assembly is ground to flat as shown in Figure 6.

As shown in Figure 7, the middle assembly consists of the middle frame, four powdered iron arcs, and a permanent magnet ring. Since a solid permanent magnet ring requires expensive customized equipment to magnetize, twelve arc-shaped permanent magnets are used instead. Each magnet is magnetized along a single direction, as illustrated in Figure 7. Therefore, the permanent arcs together can be approximated as a radially-magnetized ring. Both sides of the middle assembly are also precision ground to ensure near seamless contact between the powdered iron stator cores.

POWER AMPLIFIER

A customized 1-kW linear power amplifier is designed and constructed to supply precisely-controlled current to the magnetic actuator, as commercial switching-mode

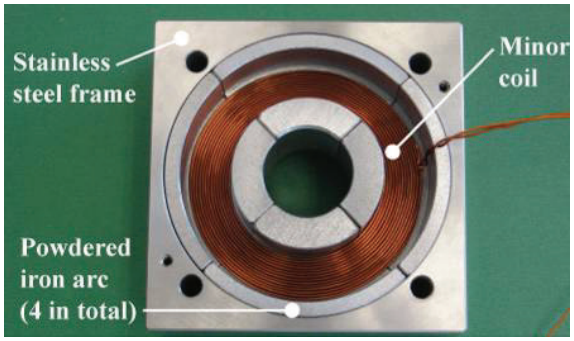

FIGURE 5: The layout of front and rear magnetic bearing assembly components.

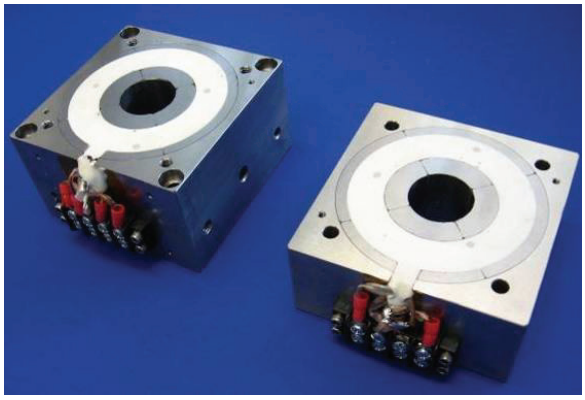

FIGURE 6: Complete front (left) and rear (right) magnetic bearing assemblies.

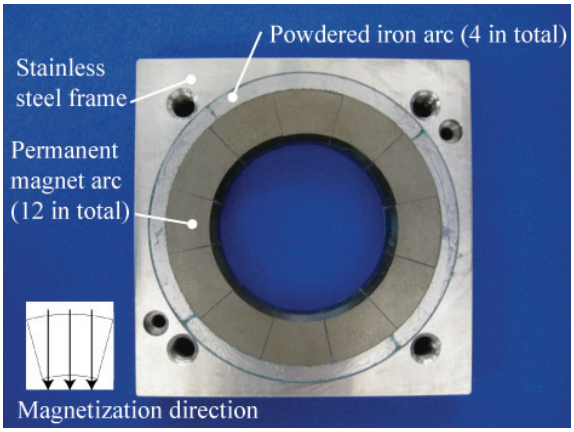

FIGURE 7: The middle bearing assembly.

amplifiers suffer from 5kHz bandwidth limit and switching noise, which can significantly deteriorates the analog position sensor performance. A cascade two loop structure is used: one inner voltage loop and one outer current control loop. Figure 8 shows the closed-loop frequency response of the power amplifier, from the current command to the actuator current. The -3dB bandwidth is about 60 kHz.

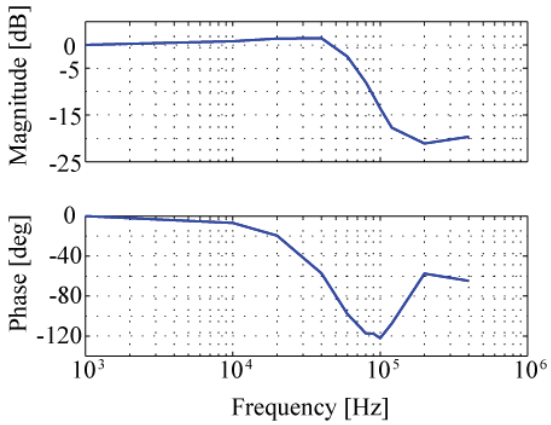

FIGURE 8: Power amplifier frequency response from the current command to the output current.

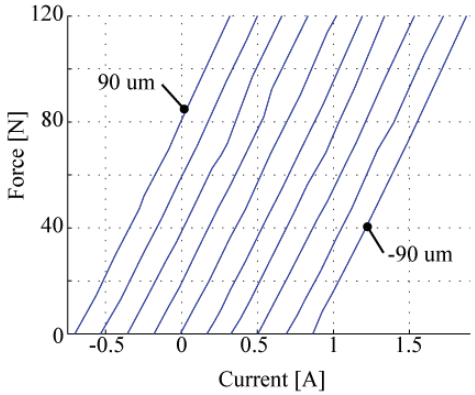

FIGURE 9: The actuator force vs. current at various constant armature positions. From left to right, the positions range from 90 μm to -90 μm in 20 μm increments.

ACTUATOR FORCE MEASUREMENT RESULTS

First, the magnetic actuator force was experimentally characterized. When holding the armature at various constant positions with a motion control loop, an external load is axially applied to the spindle front end through a digital force gauge. Recording the applied load versus actuator current at steady state gives the actuator force results shown in Figure 9. It can be seen that the actuating force changes linearly with both the armature position and the excitation current. The actuator stiffness k_x and force coefficient k_i are derived from linear fitting. Table 2 lists the comparison between the experimental measurements and the finite element analysis (FEA). The deviation of the experiment from the FEA is 20~30%. In order to investigate this discrepancy, we removed the middle assembly and then connect the rear assembly directly to the front assembly. By measuring the mutual inductance between the front stator coil to the rear stator coil, the initial permeability of the soft magnetic material was determined to be about 105~130 depending on the excitation amplitude. This permeability result is much lower than the value of 500 indicated by the manufacture-supplied B-H curve. This low permeability is consistent with the test results from vibrating sample magnetometer method [10]. As the 1.2 mm air gap constitutes a significant portion of the total reluctance, the much lower permeability of the magnetic material only results in less than 30% force reduction.

TABLE 2: Experimental results v. FEA results

	Experimental	FEA	% Difference
k_x [N/μm]	1.04	1.53	-32%
k_i [N/A]	118	147	-19.7%

AXIAL MOTION CONTROL

Using swept sine wave identification, Figure 10 shows the frequency response measurement from the actuator current command to spindle shaft axial position. The flat region at low frequency up to 120 Hz is due to the negative spring effect of the magnetic bearing, as the phase remains at -180 degree in this region. The free mass rigid-body mode shifts the magnitude response slot from 0 to -40dB/dec from 120 Hz to 1 kHz. According to (8), we can extract the bearing stiffness k_x and force coefficient k_i from the frequency response measurement. The 120 Hz corner frequency squared and multiplied by the shaft mass gives the constant k_x = 1.05 N/μm. Multiplying the DC gain of the frequency response by k_x gives k_i = 110 N/A. This confirms the previous static force measurement results.

Beyond 1 kHz, there exist a rich set of collocated resonance modes located at 1700 Hz, 2300 Hz, 2800 Hz and 3200 Hz. Using a structural finite element analysis tool COSMOS [11], we can identify the cause of the first three peaks in the frequency response as the spindle shaft bending modes weakly excited by the magnetic pressure distributed on the armature. The large resonant peak at 3200 Hz is caused by a axial vibration mode, which sets the limit of the achievable bandwidth of the axial control loop.

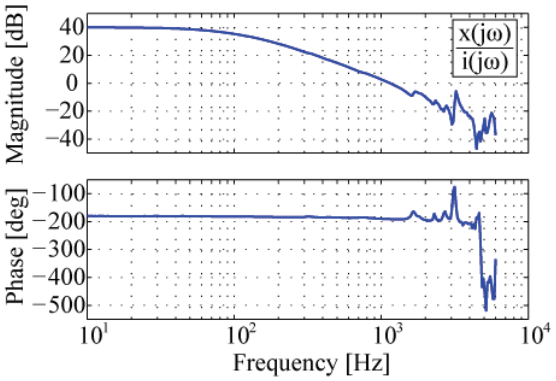

FIGURE 10: The plant frequency response from current command to axial position.

Axial Controller Design and Implementation

Having identified the plant frequency response, a loop shaping controller can be designed. The controller consists of a loop shaping term *C(s)* and an integrator, as shown in Figure 11, and *P(s)* is the plant represented by the frequency response in Figure 10. *C(s)* is used to provide sufficient phase margin near the loop transmission crossover frequency region. This is accomplished with two phase compensators to increase phase margin at the crossover frequency, and two low pass filters for high frequency roll off and resonance attenuation. The controller transfer function is:

$$C(s) = \frac{7.51e6(s+1414)(s+1728)}{(s+22619)(s+27646)(s+8796)^2} \qquad (9)$$

K_{int} is set at 560 to enhance the low frequency gain and eliminate steady-state error. The whole controller is implemented at 100 kHz sampling rate on a dSPACE DS1103.

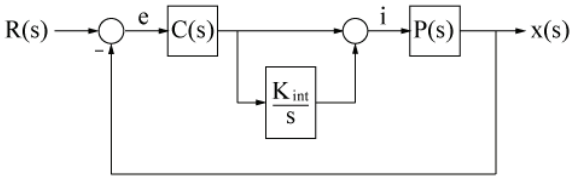

FIGURE 11: The control system block diagram.

The compensated negative loop transmission frequency response is shown in Figure 12. The unity gain crossover frequency of the loop transmission is 960 Hz with 40 degrees of phase margin.

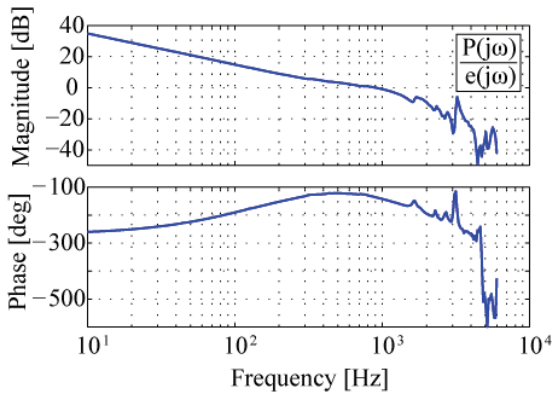

FIGURE 12: The frequency response of the negative of loop transmission.

Figure 13 shows the closed-loop response from the axial position reference command *R(s)* to the displacement sensor measurement *x(s)*. The -3dB closed-loop bandwidth is 1500 Hz. Figure 14 shows a 1-μm step response of the axial actuator under closed-loop control. The peak time is 0.5 ms (Figure 14), which closely coincides with our 960 Hz crossover frequency. For constant position regulation, Figure 15 shows the positioning noise, which is less than 5 nm RMS and zero steady state error. This noise is primarily contributed by the electrical noise of the capacitive displacement sensor.

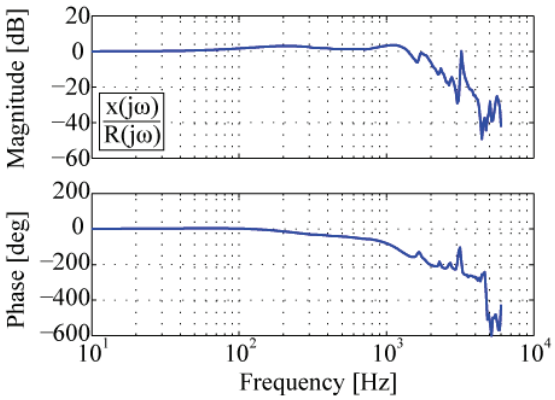

FIGURE 13: The closed-loop frequency response.

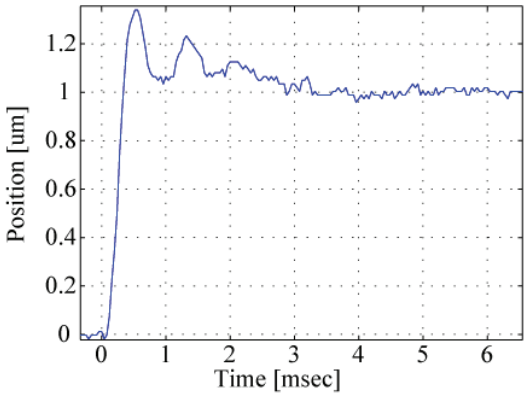

FIGURE 14: The 1-μm step response of the closed-loop system.

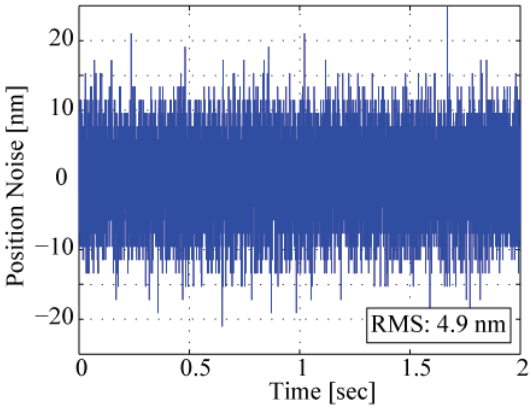

FIGURE 15: The axial loop actuator regulation noise.

SUMMARY AND OUTLOOK

A prototype radially-biased thrust magnetic bearing/actuator has been constructed and integrated into a precision spindle. Both the analytical result and the experimental measurement confirms that the actuating force is a linear function of both the armature position and the excitation current. Future work includes investigation of the machining process with such type of spindle.

REFERENCES

1. Zhang, X., Shinshi T., Endo, H., Shimokohbe, A., Imai, Y., Miyake, H., and Nakgawa, T., Micro Electrical Discharge Machining Using a 5-DOF Controlled Maglev Actuator, Proc. of ASPE 2007 Annual Meeting, 36-39, 2007.
2. Shinshi, T., Sata, K., and Shimokohbe, A., A Compact Aerostatic Spindle Integrated with an Axial Positioning Actuator for Micro and Ultra-Precision Machine Tools, Int. Journal of Automation Technologyu, Vol. 2, No. 1, 56-63, 2007.
3. Liebman, M. K., Rotary-Linear Axes for High Speed Machining, MIT PhD Thesis, 2001.
4. Studer, P.A., A Practical Magnetic Bearing, IEEE Transaction on Magnetics, Vol. 13, No. 5, 1977.
5. Molenaar, A., van Beek, H.F., and Sanders, M.J.L., A new linear magnetic bearing configuration for high accuracy positioning, Proceedings of MAG 97: Magnetic Bearing, Magnetic Drives and Dry Gas Seals Conference, 1997.
6. Murphy, B.T., Ouroua, H., Caprio, M.T., Herbst, J.D., Permanent Magnet Bias, Homopolar Magnetic Bearings for a 130 kW-hr Composite Flywheel, Proceedings of the 9th Int. Symposium on Magnetic Bearings, 2004.
7. Lu, X.-D., Trumper, D. L., Ultra Fast Tool Servos for Diamond Turning, Annals of the CIRP, Vol. 54, No. 1, pp. 383-388, 2005.
8. Meeker, D. Finite Element Method Magnetics, Version 4.2, http://femm.foster-miller.net
9. Höganäs. http://www.hoganas.com/
10. Gilbert, I., Bull, S., Evans, T., Jack, A., Effects of processing upon the properties of soft magnetic composites for low loss applications, Journal of Materials Science, Vol. 39, 457-461, 2004.
11. SolidWorks Corporation. COSMOSWorks 2007 SP3.1, www.solidworks.com